Acta Materialia 153 (2018) 391–403

Contents lists available at ScienceDirect

Acta Materialia

journal homepage: www.elsevier.com/locate/actamat

Full length article

Hardening by slip-twin and twin-twin interactions in FeMnNiCoCr

M. Bönisch [1], Y. Wu [1], H. Sehitoglu*

Department of Mechanical Science and Engineering, University of Illinois at Urbana-Champaign, 1206 W. Green St., Urbana, IL 61801, USA

ARTICLE INFO

Article history:
Received 11 January 2018
Received in revised form
14 April 2018
Accepted 24 April 2018
Available online 27 April 2018

Keywords:
High entropy alloys
Residual burgers vector
Strain softening
Slip-twin interaction
Twin-twin interaction
Latent hardening

ABSTRACT

To enhance strain hardening of alloys beyond levels accessible by forest hardening slip-twin interactions and twin-twin interactions have been proposed. The high entropy alloy FeMnNiCoCr constitutes a prominent example of exceptionally pronounced strain hardening instigated by profuse slip-twin/twin-slip and twin-twin interaction at cryogenic temperatures. In the current study, we perform uniaxial straining experiments on single crystals at 77 K. The $<144>_{Tension}$ crystal shows the potential ease of twin progression for slip-twin interaction (softening) in contrast to the difficulty for twin advancement in $<122>_{Tension}$, $<111>_{Tension}$ and $<001>_{Compression}$ cases (hardening). The corresponding self and latent hardening coefficients derived from the data reveal that slip-twin latent moduli are much smaller than twin-twin latent moduli. Unlike previous undertakings, this study demonstrates a novel approach to assess latent hardening where plastic straining is implemented in a monotonic fashion and primary and latent systems operate simultaneously. To predict the flow stress depending on crystal orientation and as a function of strain a numerical model is proposed using the obtained hardening moduli. It emerges that the magnitude of residual Burgers vectors originating from twin-related reactions can explain the experimental hardening/softening trends. These results hold considerable promise for a quantitative description of strain hardening in metals and alloys.

1. Introduction

1.1. Background and objectives

Deformation twinning is the most widespread mechanism to accommodate plastic strain in metallic materials aside from crystallographic slip. Since the early observation of twinning in FCC (face-centered cubic) materials [1], there have been numerous studies investigating the interactions between slip and twin [2–7]. These interactions play a decisive role for the strain hardening behavior, inasmuch they significantly affect the slope of the stress-strain curve after yielding - i.e. the strain hardening rate. The underlying mechanism can be attributed to the introduction of twin interfaces. Similar to a grain boundary, a twin interface can serve as formidable obstacle to the motion of impinging dislocations. Glissile and sessile dislocations originating from the reaction of incoming dislocations at the interface inevitably affect both strength and ductility. In the majority of studies, twin-slip and twin-twin interactions were found to strengthen (strain-harden) the material effectively [8,9]. However, in some cases the associated mechanical responses can exhibit no hardening [10,11] or even strain-softening [12–14], despite considerable slip and twin activities. A conclusive rationalization for this seeming discrepancy is still to be put forward and, therefore, the purpose of this paper is to examine this very concern.

For the present case study, we use the equi-atomic FeMnNiCoCr high entropy alloy (HEA) in singe-crystalline form, which falls into the general category of low stacking fault energy (SFE) FCC alloys such as Hadfield steels [15], Co-Ni [16,17] and Cu-Al alloys [18]. Incurred by the low SFE deformation twins have been reported for FeMnNiCoCr when strained at cryogenic temperature (77 K) [19–21]. To effectively elucidate the interaction-controlled mechanical response we chose to illustrate 3 situations exhibiting contrasting interactions and hardening: Case 1: twin-slip hardening, Case 2: twin-slip softening and Case 3: twin-twin hardening. We observed pronounced twin-twin interaction for

* Corresponding author.
E-mail address: huseyin@illinois.edu (H. Sehitoglu).
[1] Equal contribution.

https://doi.org/10.1016/j.actamat.2018.04.054
1359-6454/

<001>$_{Compression}$ and <111>$_{Tension}$ loading cases, contrary to slip-twin/twin-slip interaction in <122>$_{Tension}$ and <144>$_{Tension}$. The stress-strain responses for these four orientations vary distinctively: the deformation twin interfaces create conditions that produce hardening in some cases (<001>$_{Compression}$, <111>$_{Tension}$ and <122>$_{Tension}$) opposed to softening in others (<144>$_{Tension}$).

The mechanical response of a polycrystalline material is affected by many-fold factors invoked by its aggregate nature: (i) formation of dislocation pile-ups at grain boundaries [19,20], (ii) dislocation reactions taking place at grain boundaries [22], (iii) the distribution of grain orientation and size, and (iv) compatibility constraints arising from the matrix. The combination of these factors cloaks contributions of individual hardening mechanisms and indisputably complicates any hardening analysis making the identification of the governing processes a challenging task. Such difficulties can be significantly mitigated by studying single crystals in which the effect of grain boundaries and the associated complications in the deformation analysis are removed. Furthermore, number and type of systems (twin and slip) activated in a single crystal are finite permitting selective isolation of interactions. Thus, one can clearly write dislocation interactions a priori based on Schmid factor considerations for the single crystal cases (provided the material obeys Schmid's law) in contrast to polycrystals. Consequently, it is feasible to pinpoint the activated systems and their mutual interactions by using single crystals permitting further analysis of the corresponding hardening and softening response.

1.2. Mechanisms associated with strain-hardening and strain-softening

In the absence of twinning strengthening of metallic materials is closely related to the forest dislocation density (Taylor's hardening model). In the case of FeMnNiCoCr, dislocation hardening governs the stress-strain response at RT at low strain while twinning plays a key role at cryogenic temperature from the very early stage of deformation on [20]. It has been recognized that at RT deformation twinning can become dominant at relatively high strains of about 25% axial strain [20]. Earlier literature notes that the significant strengthening of (nano-)twinned materials (e.g. nano-twinned Cu and NiCo) can be attributed to the presence of twin interfaces [23,24]. Upon mechanical twinning, the dynamic Hall-Petch effect provides a plausible rationalization for material strengthening as the introduction of new interfaces due to twinning reduces the dislocation mean free path. Numerous studies using transmission electron microscopy (TEM) have confirmed the formation of dislocation pile-ups at the twin interfaces, justifzing their role as barrier to dislocation motion [9]. In addition, many theoretical studies using molecular dynamics (MD) simulation have been ventured to reveal the underlying mechanisms [5,24–26]. As a dislocation impinges and interacts with a barrier twin boundary, it is suggested that the incident dislocation can either incorporate into or block by or transfer through the twin boundary [5,25]. An important outcome of these dislocation reactions is the creation of residual Burgers vectors, which can serve as obstacles to dislocation glide on the twin boundary. Their magnitude can be indicative of the strain hardening level. In the current study, we show that the magnitude of residual dislocations formed by slip-twin interactions are smaller than those by twin-twin interactions, which complies with the experimental trend.

Compared to strain-hardening, which has been investigated by many studies for a large variety of materials, fewer works were endeavored to explain the lack of hardening or even strain-softening in alloys. For example, in Hadfield steel (Fe-Mn-C) the plastic flow proceeds at nearly constant stress in the range of 0–20% and 0–10% when loaded along <144> and <111> in tension, respectively [10]. Such behaviors are usually accompanied by the formation of Lüders bands during deformation in experiments [11]. Several mechanisms have been proposed from foregoing undertakings using MD simulations to rationalize such phenomena, especially those associated with strain-softening. It has been revealed that the stacking-fault nucleation energy barrier can be much smaller than the twin migration energy barrier in some materials, e.g. Pd [13]. In this case, the twin boundary acts as a dislocation source and the nucleation and motion of partial dislocations parallel to the twin boundary is energetically favorable, which can eventually lead to detwinning and, thereby, to flow softening. Furthermore, it was suggested that the twin thickness and twin boundary spacing are crucial and responsible for the softening response in nano-twinned metals [14]. A recent work on nano-twinned Cu [12] revealed that defects, such as kink-like steps and curvature, contained in a coherent twin boundary can further facilitate flow softening. In this study, we found more experimental evidence for strain softening behavior in <144>$_{tension}$ oriented FeMnNiCoCr. The underlying mechanism is rationalized by a combined effect of strain localization and small residual Burgers vector.

1.3. Determination of self and latent hardening moduli

Strain hardening and softening are complicated phenomena and correlating them to the underlying deformation mechanisms and interactions (slip, twin, or mixed) remains a challenging endeavor [27,28]. In a single crystalline material, mutual interactions between different deformation systems are expected to dominate the flow stress evolution. The change of the flow stress on each system can be resolved into self hardening of the active system(s) combined with latent hardening, which measures the increase or decrease of the resistance to plastic deformation on latent systems by shearing the primary system [29]. Heretofore, a quantitative analysis of these hardening moduli has been rarely performed although their accurate determination is crucial for predictive crystal plasticity modeling free from fit parameters. The present paper can be deemed as an important and necessary effort taking up this very matter.

Inspired by early works by Mandel [30] and Hill [31], a crystal plasticity framework, idealized as time independent and incorporating contributions from pure slip, pure deformation twinning and mixed interactions (slip-twin, twin-slip) to the strain hardening, may be written as follows:

$$\begin{aligned} d\tau_i^{crit} = & \underbrace{\left(1-\sum_k^N f_k{}^{tw}\right)\sum_j^N h_{ij}^{s-s} d\gamma_j^s}_{\text{slip}-\text{slip}} + \underbrace{\sum_j^N df_j{}^{tw} h_{ij}^{s-tw}\gamma^{tw}}_{\text{slip}-\text{twin}} \\ & + \underbrace{\left(1-\sum_k^N f_k{}^{tw}\right)\sum_j^N h_{ij}^{tw-s} d\gamma_j^s}_{\text{twin}-\text{slip}} + \underbrace{\sum_j^N df_j{}^{tw} h_{ij}^{tw-tw}\gamma^{tw}}_{\text{twin}-\text{twin}} \end{aligned} \quad (1)$$

where $d\tau_i^{crit}$ is the change of flow stress on the i-th system, $f_k{}^{tw}$ denotes the volume fraction of the k-th twin system, γ_j^s is the shear strain of the j-th slip system, γ^{tw} is the intrinsic twin shear strain for FCC (0.707), andh_{ij}^{s-s}, h_{ij}^{s-tw}, h_{ij}^{tw-s} and h_{ij}^{tw-tw} represent the strain hardening coefficients (moduli) associated with slip-slip, slip-twin, twin-slip and twin-twin interaction, respectively. At this point we

would like to draw the reader's attention to the difference between slip-twin vs. twin-slip interactions, which is vital for the following hardening description. In the modulus notation employed, the first index (superscript) specifies the secondary (latent) system and the second index (superscript) the primary system. Thus, the slip-twin moduli h_{ij}^{s-tw} characterize the latent hardening of slip by twinning and, vice versa, the twin-slip moduli h_{ij}^{tw-s} the latent hardening of twins by slip.

Although there has been some efforts on extracting hardening moduli from polycrystalline materials [32,33], they can only reflect effective values as the distinction between individual interactions from the corresponding stress-strain curve is rather vague. However, the determination of each hardening modulus can be facilitated using differently oriented single crystals where the deforming systems and their interactions can be accurately identified. For example, we confirmed twin-twin activities for both $<001>_{Compression}$ and $<111>_{Tension}$ and slip-twin/twin-slip interactions for $<122>_{Tension}$ and $<144>_{Tension}$. The corresponding h_{ij} values can be evaluated using the relevant section of the experimental stress-strain curve for the specific pair of interaction. We will elaborate on the calculation procedure in Section 3.5. Note that when i represents a slip system, the last two terms in Equation (1) do not appear. Vice versa, when i represents a twin system, the first two terms in Equation (1) can be ignored.

It is important to point out that to determine the (latent and self) hardening moduli in this work we demonstrate a novel approach where the sample is strained in a continuous manner and the moduli are obtained under the condition where both primary and latent systems are active. In foregoing undertakings, so-called 'latent hardening experiments' were performed [29,34–39]. In this setting, a primary system was first nucleated via deforming the crystal in its pristine state. Then, a previously inactive system was activated by straining a new sample cut from the pre-deformed crystal at specific angles. The hardening of the latent system was then assessed from the latent hardening ratio (LHR) which relates the critical (yield) stress for the secondary test to the maximum stress measured during the primary test. This indirect measurement has proven very instructive and results obtained thereof have been frequently implemented in crystal plasticity modeling [40]. However, the change of crystal orientation can create a fairly unnatural situation as the primary system is deliberately suppressed by lowering its Schmid factor. Therefore, the previous methodology represents a rather idealized scenario. In the present study, the plastic deformation proceeds in a monotonic fashion to large strains whereby both primary and latent systems remain active throughout. We believe that this newly established approach eliminates the need for crystal-reorientation while allowing determination of the strain hardening levels without ambiguity.

Using high resolution digital image correlation (DIC) and electron backscatter diffraction (EBSD) the activated slip and twin systems are identified complemented by transmission electron microscopy of the interactions between different deformation systems. Finally, we calculate the hardening moduli h_{ij} based on the experimental results for all loading cases where the deformation systems are unambiguously identified. For the characterization of slip hardening, dislocation densities were measured to support the calculations. From the hardening moduli obtained the flow stresses were then computed at various strains and the predictions were compared to the experimental results. The LHRs will be derived from the hardening moduli and illustrated. In parallel, the magnitude of the residual Burgers vector $|\underline{b}^r|$ formed by the observed twin-twin and slip-twin interactions are calculated. We find that the corresponding $|\underline{b}^r|$ varies with interaction type and involved systems and it is indicative of the associated hardening. The results reveal that the hardening associated with slip-twin interactions is smaller than that associated with twin-twin interactions.

Table 1
Designations of the 12 twin systems of an FCC crystal subjected to tension along $<111>_T$, $<122>_T$ and $<144>_T$ and to compression along $<001>_C$ nominal loading directions. The Schmid factors are calculated based on the exact crystal orientations determined from EBSD. The activated twin systems of each case are highlighted in the table.

No.	Twin system	Schmid factor (m)			
		$<111>_T$	$<100>_C$	$<122>_T$	$<144>_T$
1	$(\bar{1}\bar{1}1)[\bar{1}\bar{1}2]$	−0.12	−0.23	−0.11	−0.20
2	$(1\bar{1}1)[1\bar{1}\bar{2}]$	−0.19	−0.25	−0.09	−0.10
3	$(\bar{1}11)[\bar{1}1\bar{2}]$	−0.23	−0.25	−0.22	−0.26
4	$(1\bar{1}1)[121]$	−0.11	−0.23	−0.04	−0.02
5	$(\bar{1}\bar{1}1)[\bar{1}21]$	0.13	−0.24	**0.30**	0.37
6	$(111)[1\bar{2}1]$	−0.09	−0.24	−0.05	−0.02
7	$(\bar{1}11)[\bar{1}\bar{2}1]$	**0.40**	−0.23	0.48	**0.49**
8	$(\bar{1}11)[211]$	−0.18	**0.47**	−0.27	−0.24
9	$(\bar{1}\bar{1}1)[2\bar{1}1]$	−0.01	**0.47**	−0.19	−0.17
10	$(1\bar{1}1)[\bar{2}\bar{1}1]$	**0.30**	0.48	0.12	0.12
11	$(111)[\bar{2}11]$	−0.12	**0.48**	−0.15	−0.07
12	$(111)[11\bar{2}]$	0.21	−0.23	0.20	0.09

2. Experimental methods

Single crystals of equiatomic FeMnNiCoCr were grown in an inert gas environment via the Bridgman technique. The ingots were first homogenized at 1473 K for 24 h followed by quenching in water. Then, solution-treatment was performed at 1373 K for 1 h followed by quenching in oil. Samples for compressive and tensile testing were cut with their loading orientations aligned along <111>, <001>, <144> and <122> directions. These orientations have been confirmed using EBSD. All uniaxial tensile ($<111>_{Tension}$, $<144>_{Tension}$ and $<122>_{Tension}$) and compressive ($<001>_{Compression}$) experiments were performed at liquid nitrogen temperature (77 K). Hereafter, the crystallographic orientations are denoted as $<111>_T$, $<122>_T$, $<144>_T$, and $<001>_C$. The loading and unloading process was achieved under strain and load control, respectively, with the sample, grips, and extensometer fully submersed in liquid nitrogen. The extensometer readout was used for constructing stress-strain curves. Since the liquid nitrogen bath does not allow in-situ DIC, DIC was performed ex-situ at room temperature. To this end, multiple load increments were performed. Before deformation, reference images were taken using an optical microscope with 10× magnification, which corresponds to a spatial resolution of 0.44 μm × 0.44 μm/pixel. To enlarge the effective field of view, 15 images were captured over an area of 3 mm × 1 mm. At the end of each load increment, the sample was removed from the load frame and the images of the deformed state were taken in the exactly same fashion. The correlation of each pair of reference and deformed images was performed using the commercial Vic-2d software with a subset size of (35 pixel × 35 pixel). The results were then stitched together as described previously [41]. It is important to note that the flatness of the sample surface can no longer be sustained after severe deformation, which can lead to substantial difficulties in taking focused DIC images under the optical microscope. Therefore, it is necessary to re-establish a flat surface via polishing after each load increment. For this reason, the DIC strain contours depicted in this paper do not necessarily

Table 2
Designations of all 12 slip systems in an FCC crystal. The Schmid factors correspond to the exact loading orientation determined from EBSD. Systems activated are highlighted.

No.	Slip system	Schmid factor (m)			
		$<111>_T$	$<100>_C$	$<122>_T$	$<144>_T$
1′	$(\bar{1}\bar{1}1)[011]$	0.14	0.01	0.23	**0.33**
2′	$(1\bar{1}1)[0\bar{1}\bar{1}]$	0.05	0.01	0.03	0.05
3′	$(\bar{1}11)[\bar{1}0\bar{1}]$	0.03	0.42	0.03	0.01
4′	$(1\bar{1}1)[\bar{1}01]$	0.28	0.42	0.13	0.12
5′	$(\bar{1}\bar{1}1)[101]$	0.06	0.40	0.05	0.02
6′	$(111)[\bar{1}01]$	0.19	0.40	0.20	0.09
7′	$(1\bar{1}\bar{1})[0\bar{1}1]$	0.33	0.41	0.43	0.43
8′	$(\bar{1}11)[\bar{1}\bar{1}0]$	0.36	0.01	**0.40**	0.44
9′	$(\bar{1}\bar{1}1)[1\bar{1}0]$	0.08	0.41	0.27	0.32
10′	$(1\bar{1}1)[\bar{1}\bar{1}0]$	0.24	0.41	0.09	0.08
11′	$(111)[1\bar{1}0]$	0.02	0.41	0.06	0.03
12′	$(111)[0\bar{1}1]$	0.17	0.01	0.14	0.06

represent the overall accumulated strain, but the strain accumulation within the corresponding load increment.

To permit an effective discussion the 12 twin and 12 slip systems for FCC were labeled according to Tables 1 and 2. The corresponding Schmid factors (m) are based on the crystal orientations measured by EBSD. The exact crystallographic orientations were identified as [0.9998 -0.0204 -0.0012], [0.5791 0.4640 -0.6703], [-0.6276 -0.1763 0.6527] and [0.7081 0.2991 -0.6397], which are denoted as $<001>_C$, $<111>_T$, $<144>_T$ and $<122>_T$ throughout the remainder of this paper. We observed that the deformation is characterized by twin-twin interactions in $<001>_C$ and $<111>_T$ cases and by slip-twin/twin-slip interactions in $<122>_T$ and $<144>_T$ cases.

Lamella for transmission electron microscopy (TEM) were extracted from strained samples perpendicular to the loading direction and thinned by focused ion beam with a FEI Helios 600i DualBeam. A JEOL 2010 LaB_6 TEM was used to identify active slip and twin systems and to image dislocations and twins. The activated slip and twin systems identified on the basis of DIC trace analysis, EBSD and TEM are highlighted in the tables. We like to point out that most slip in FeMnNiCoCr occurs by glide of full dislocations, as illustrated by Burgers vector analysis using TEM (Fig. A1(a) in the Appendix) and TEM images of deformed microstructures in other studies [19,20,42]. Accordingly, the slip Schmid factors in Table 2 are those for full FCC dislocations.

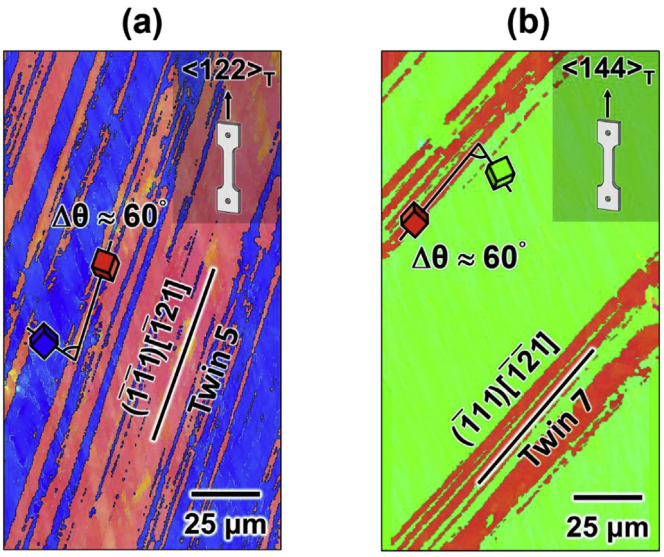

Fig. 2. EBSD orientation maps of single crystals oriented strained in tension to ~11% along (a) $<122>_T$ and (b) $<144>_T$.

3. Experimental results

3.1. Stress-strain responses

Fig. 1 illustrates the mechanical responses (up to ~11% of strain) of the chosen single crystals deformed at 77 K with the ex-situ DIC

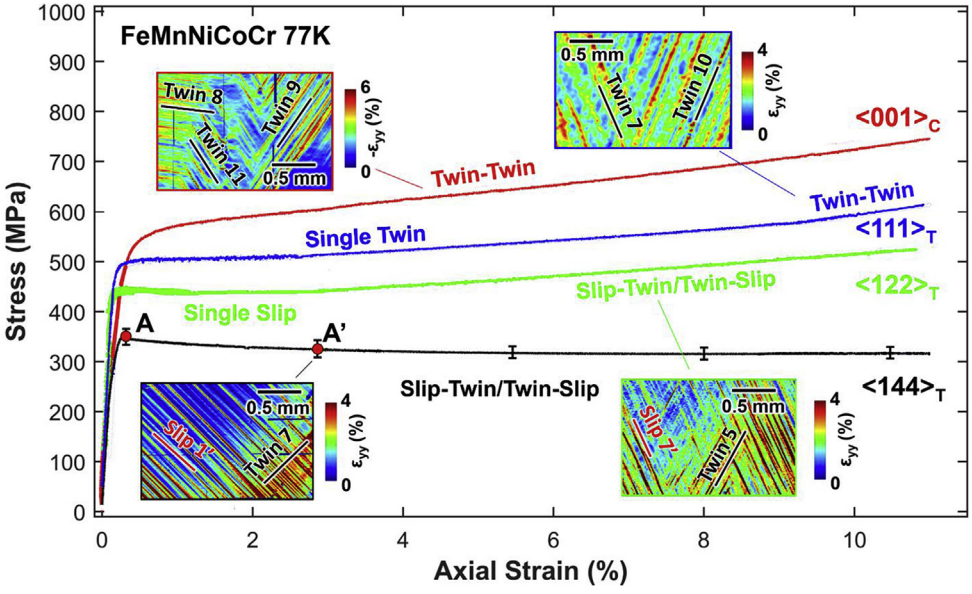

Fig. 1. The mechanical responses of single crystals oriented along $<001>_C$ $<111>_T$, $<122>_T$ and $<144>_T$ together with select DIC strain contours. Error bars for the $<144>_T$ case demonstrate the reproducibility of the softening behavior.

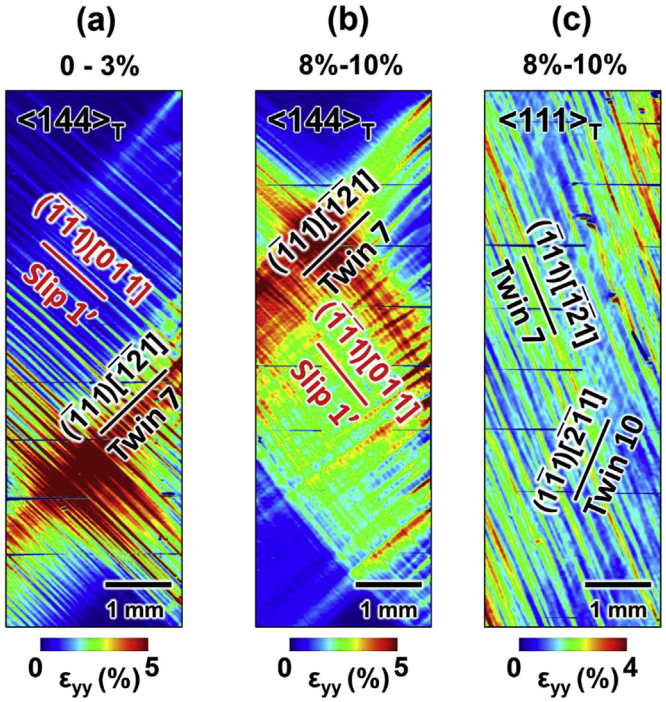

Fig. 3. Full-field (3 mm × 10 mm) strain contours at different axial strain intervals. The images illustrate the spatial strain distribution for (a) the $<144>_T$ case from 0 to 3% strain, (b) the $<144>_T$ case from 8 to 10% strain and (c) the $<111>_T$ case from 8 to 10% strain.

strain contours showcased for each loading orientation. The localized DIC bands correspond to twin or slip systems which were identified via trace analysis. For example, in the $<144>_T$ case, the localized strain bands match with the intersections of the $(\bar{1}11)$ and $(\bar{1}\bar{1}1)$ planes with the sample surface. Then, due to their high Schmid factors, the activated systems were identified as $(\bar{1}11)[0\bar{1}1]$ (slip 1′, $m = 0.33$) and $(\bar{1}\bar{1}1)[\bar{1}2\bar{1}]$ (twin 7, $m = 0.49$). In the $<122>_T$ case, deformation was accommodated by a single slip system (slip 7′, $m = 0.40$) at small strains and the nucleation of a secondary twin system (twin 5, $m = 0.30$) ensued at higher strains. When considering the $<111>_T$ single crystal, it is evident that a primary twin system (twin 7, $m = 0.40$) became active at the early stage of deformation followed by a secondary twin system triggered at ~ 8% of axial strain (twin 10, $m = 0.30$). For $<001>_C$ three twin systems were found to become active almost simultaneously due to their similar Schmid factors (twin 8, $m = 0.47$; twin 9, $m = 0.47$; twin 11, $m = 0.48$). The twin systems observed were further corroborated by additional EBSD and TEM analysis in each case, which is an important step for the hardening analysis. We show the EBSD orientation maps for the $<122>_T$ and $<144>_T$ cases in Fig. 2 to justify our observation.

From Fig. 1, the twin nucleation stress, determined with 0.1% offset, is 410 ± 10 MPa in the $<111>_T$ case and 420 ± 10 MPa in the $<001>_C$ case, which correspond to critical resolved shear stresses (CRSS) of 164 ±4 MPa and 197 ±5 MPa. The resultant averaged CRSS for twinning is approximately 180 MPa, in agreement with theory [43]. Similarly, the slip nucleation stress, determined with 0.1% offset, is 380 ± 10 MPa and 350 ± 10 MPa in the $<122>_T$ case and the $<144>_T$ case, respectively. The associated CRSS for slip 7′ and slip 1′ is 163.4 ± 4 MPa and 154 ± 4 MPa, which gives an averaged value of approximately 159 MPa in very good agreement with previously reported values [21].

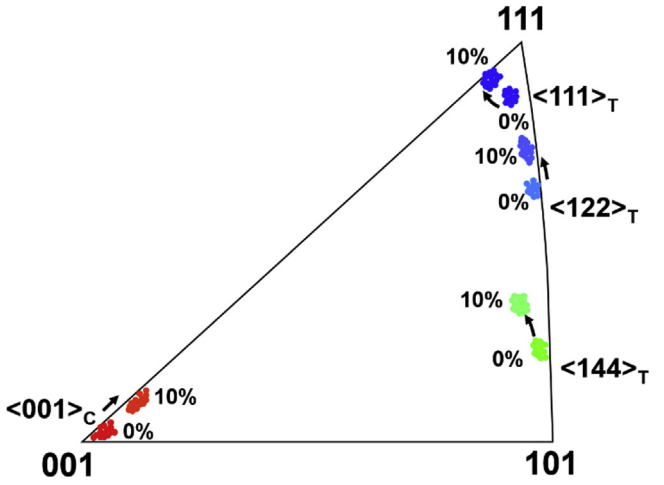

Fig. 4. Evolution of loading direction for each crystal orientation from 0% to ~10% axial strain.

It is evident from Fig. 1 that the strain hardening slope, $d\sigma/d\varepsilon$, associated with twin-twin interaction is significantly higher than that for slip-twin/twin-slip interaction. For example, when a single crystal is strained along $<001>_C$, $d\sigma/d\varepsilon$ can reach an order of ~3 GPa as shown in Fig. 1. This value exceeds the hardening slope of slip-twin/twin-slip interactions for $<122>_T$ (~0.5 GPa) and $<144>_T$ cases (~-0.62 GPa) by far. In particular the $<144>_T$ case shows an unusual strain softening response. This softening behavior was validated with multiple experiments as the error bars in Fig. 1 demonstrate. A plausible explanation for the unusual stress-strain response are residual dislocations ($\underline{b}^r$) left behind at interactions sites on twin boundaries, which we will discuss later on (Section 5.2). The residuals modify the twin migration energy barrier which results in raising the twin stress in some cases and lowering it in others. At the outset, we should point out that twin-twin interactions result in rather long residual Burgers vectors which translate into considerable strain hardening, while under slip-twin interactions the residual Burgers vectors are much shorter. We will elaborate on this result in the next section.

Furthermore, upon examination of the full field DIC strain contours we discovered pronounced differences in strain localization for the $<144>_T$ case compared to the others (the $<111>_T$ loading case is shown here). Fig. 3 illustrates the strain contour over the entire gauge section for the $<144>_T$ and $<111>_T$ loading cases. Note that with the migration of the twin from low to high strain level, the strain localization moves from the bottom to the top of the sample in the $<144>_T$ case. Such behavior can also be related to the unusual strain softening behavior associated with the $<144>_T$ case.

Fig. 4 illustrates the change of loading direction for each of the four single crystal orientations upon deformation to an axial strain of 10%. The Schmid factors for the activated systems were re-established based on the updated crystal orientations and the results are tabulated in Table 3. Note that comparing the Schmid factors at ~10% of strain to those of the pristine crystals (Tables 1 and 2) evidences rather small differences. Also, we emphasize that the exact orientations measured by EBSD were used in Schmid factor calculations (initial vs. strained) but for simplicity we designate them nominally as $<001>_C$, $<111>_T$, $<122>_T$ and $<144>_T$.

Table 3
The updated Schmid factors for the activated systems based on the loading orientations at ~10% axial strain.

Nominal orientation	Activated systems	Schmid factor at ~10% strain
$<001>_C$	Twin 8	0.47
	Twin 9	0.44
	Twin 11	0.47
$<111>_T$	Twin 7	0.36
	Twin 10	0.34
$<122>_T$	Slip 7′	0.41
	Twin 5	0.29
$<144>_T$	Slip 1′	0.34
	Twin 7	0.49

3.2. Examination of residual Burgers vectors

We calculated the magnitudes $|\underline{b}^r|$ of the residual Burgers vectors generated at the twin boundaries for possible interactions between the observed active slip and twin systems; Table 4 provides a summary. At the outset, we should point out that twin-twin interactions result in rather high residual Burgers which translate to considerable strain hardening, while under slip-twin interactions the residual Burgers vector magnitudes are much lower. These residuals represent debris left behind at the interaction site inasmuch they are incoming dislocation components unable to transfer across the boundary or glide away from the interaction site. Only the most plausible reactions resulting in low $|\underline{b}^r|$ [44] and minimal line energy (estimated by Frank's criterion [45]) are included in Table 4. $|\underline{b}^r|$ of the twin-twin interactions ranges from $0.59a$ to $1.22a$, where a is the lattice constant of FeMnNiCoCr. It is evident that the $|\underline{b}^r|$ values of twin-twin cases are higher than that of slip-twin cases ($0.47a$). Comparing $|\underline{b}^r|$ with the attendant hardening reveals a clear correlation of the residual's length with the degree of hardening (that is to say $d\sigma/d\varepsilon$) observed in the uniaxial experiments (see also Section 3.6). The calculation of $|\underline{b}^r|$ produced from twin-twin and slip twin interactions is showcased below.

More details on the calculation of $|\underline{b}^r|$ for twin-twin interaction can be found elsewhere [42]. For a crystal loaded along $<001>_C$, the activated twinning systems are identified as $(\bar{1}\bar{1}1)[2\bar{1}1]$ and $(111)[\bar{2}11]$. The former is denoted as Twin 9 and the latter Twin 11 as shown in Table 4. The calculation of the residual Burgers vector needs to be carried out in the same coordinate frame and the corresponding coordinate transformation can be expressed as the following:

$$\frac{a}{6}\left[\bar{2}11\right]_{T11} \rightarrow \frac{a}{18}[2\bar{5}\bar{5}]_{T9} \tag{2}$$

Based on earlier analysis [46], the generation of a full step on the barrier twin boundary requires the incorporation of triplets of incident twinning dislocations. Therefore, the reaction between Twin 9 and Twin 11 in an incorporation scenario can be written as Equation (3) and the corresponding $|\underline{b}^r|$ is 0.94a.

$$\underset{\text{incident}}{3 \times \frac{a}{6}\left[2\bar{1}1\right]} \rightarrow \underset{\text{barrier}}{\frac{a}{18}[2\bar{5}\bar{5}]} + \underset{\text{residual}}{\frac{1}{9}\left[8\bar{2}2\right]} \tag{3}$$

For a $<122>_T$ oriented crystal deformed in tension, $(1\bar{1}\bar{1})[01\bar{1}]$ slip and $(\bar{1}\bar{1}1)[\bar{1}21]$ twin modes are active (as demonstrated in Fig. 1) and the $[01\bar{1}]$ dislocations will inevitably interact with the twins boundaries. First, the full dislocation would dissociate into two Shockley partials as follows,

$$\underset{\text{full}}{\frac{a}{2}\left[01\bar{1}\right]} \rightarrow \underset{\text{leading}}{\frac{a}{6}\left[12\bar{1}\right]} + \underset{\text{trailing}}{\frac{a}{6}\left[\bar{1}1\bar{2}\right]} \tag{4}$$

Then, upon interaction, the incident leading dislocation is incorporated into the existing twin forming a twin partial on the boundary and a residual dislocation. The reaction can be summarized as follows:

$$\underset{\text{leading}}{\frac{a}{6}\left[12\bar{1}\right]} \rightarrow \underset{\text{twin partial}}{\frac{a}{6}\left[\bar{1}21\right]} + \underset{\text{residual}}{\frac{a}{3}\left[10\bar{1}\right]} \tag{5}$$

In this case, no transmission occurs as the residual dislocation, $\frac{a}{3}[10\bar{1}]$, remains sessile with no further dissociation. The magnitude of the residual Burgers vector is $0.47a$. Further interaction between the trailing dislocation and this residual dislocation can lead to different scenarios [5,6]. However, the ensuing magnitude of the residual dislocation and line energy of the reaction products increase in this process rendering the reaction of the trailing less plausible compared to Equation (5). For a single crystal oriented in $<144>_T$ crystallographic direction a similar reaction occurs, albeit with different signs, and the same residual ensues.

3.3. Twin-related interactions studied by TEM

We further illustrate the characteristics of the 3 interaction modes evidenced by DIC (twin-slip, slip-twin and twin-twin) by TEM, as shown in Fig. 5. Twins interacting with primary slip (twin-slip, Fig. 5(a)) shear the pre-existing slip bands resulting in kinked slip bands. Because of the absence of barrier interfaces no residual dislocations are formed in this process. Limited hardening may still entail due to the primary dislocations hindering the twin front (or boundary) to advance freely. On the other hand, twins approaching other non co-planar twins (twin-twin, Fig. 5(b)) may get arrested at the barrier interface. As demonstrated in previous studies [3,5] the incoming twinning dislocations may transfer into the barrier twin system, leaving behind residual dislocations. Thus, plasticity is effectively conveyed to the barrier (secondary) system.

Aside from forming barriers, twin boundaries may act as favorable nucleation sites for dislocations and secondary twins [13,47]. Their potency for diverting (and thereby delocalizing)

Table 4
Magnitudes of the residual Burgers vectors $|\underline{b}^r|$ for the observed slip-twin and twin-twin interactions depending on the loading orientation. a is the lattice constant of FeMnNiCoCr.

Loading direction	Incoming system	Barrier system	Residual Burgers vector ($|\underline{b}^r|$)
$<144>_T$	Slip 1′	Twin 7	$0.47a$
$<122>_T$	Slip 7′	Twin 5	$0.47a$
$<111>_T$	Twin 7	Twin 10	$0.70a$
$<001>_C$	Twin 9	Twin 8	$0.59a$
	Twin 9	Twin 11	$0.94a$
	Twin 8	Twin 11	$1.22a$

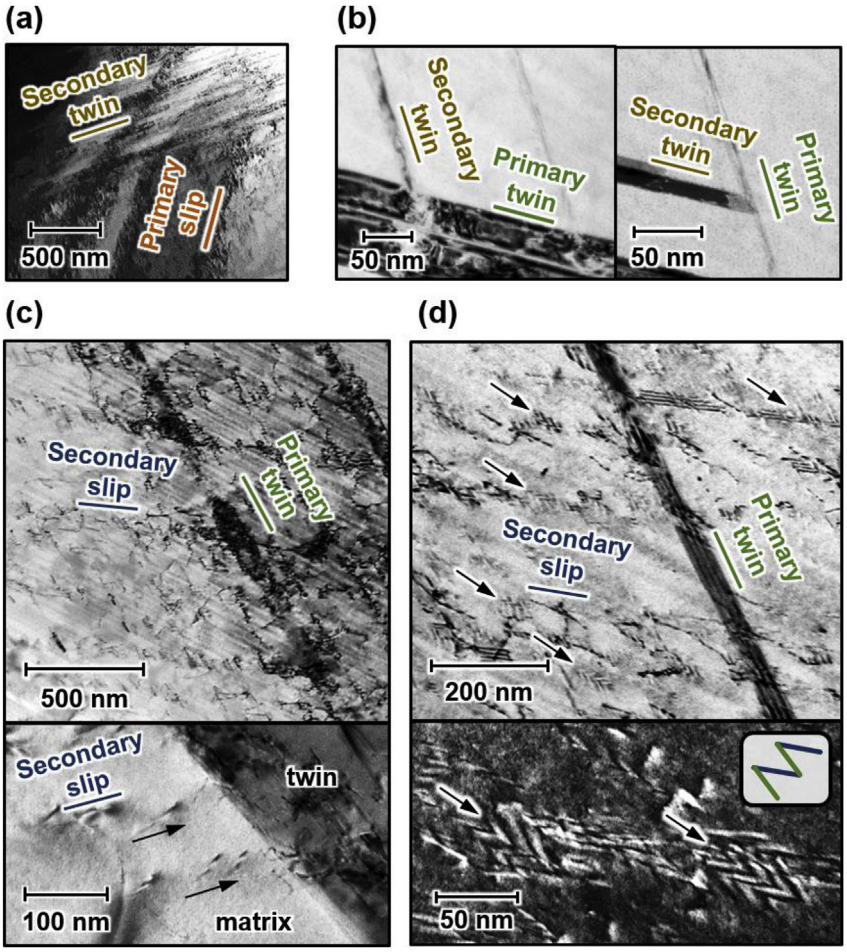

Fig. 5. Examples for twin-related interactions in FeMnNiCoCr observed by TEM illustrating (a) twin-slip, (b) twin-twin and (c,d) slip-twin mechanisms. Arrows in the close-up view in (c) indicate the assumed direction of lattice dislocation motion. (d) Several interlocked stacking faults are marked and the dark-field image shows the resulting chevron fringe pattern in detail. The traces of primary and secondary twin/slip system are indicated in the inset.

plasticity is thus two-fold. Yet, while central to their role as barriers are residual dislocations and the attendant hardening, when acting as nucleation sites their initial role is to simply promote plasticity by delocalizing it. Hardening will then still occur when the primary twin remains active and transfers following twinning dislocations onto the nucleated system.

Transfer of slip may occur in a similar manner when lattice dislocations impinge on a barrier twin boundary. Fig. 5(c) and (d) demonstrate examples of slip interacting with twin boundaries (slip-twin). For the most part, the lattice dislocations contributing to slip such as those in Fig. 5(c) exhibit full character as demonstrated by the Burger vector analysis in Fig. A1(a) in the appendix. However, due to the low stacking fault energy of FeMnNiCoCr [18] extended dislocations giving rise to stacking fault ribbons were observed, too, yet at a much lower rate than undissociated (full) dislocations. Faults occurred both on planes belonging to primary and secondary systems and we observed cases where their interaction led to chevron-type patterns, as shown in the magnified dark-field view in Fig. 5(d). These features resemble a series of Lomer-Cottrell locks where at each apex a sessile, locking dislocation holds the stacking fault ribbons extending from it in place.

The nature of the stacking faults was determined as intrinsic as revealed in Fig. A1(b). The presence of intrinsic stacking faults, which can be considered as precursors to twins, attests to the increased twin propensity of FeMnCoCrNi at low temperature. Still, it is important to point out that lattice dislocations observed are overwhelmingly full dislocations.

3.4. Determination of strain hardening coefficients (h_{ij})

In this section, we demonstrate the calculation procedure for the latent and associated self hardening moduli for slip-twin/twin-slip interactions on the basis of the <144>$_T$ case. For this orientation interaction between slip system 1′ and twin system 7 is evident (Figs. 1–3) and the governing Equation (1) can be modified into

$$d\tau_{1'}^{crit} = h_{1'1'}^{s-s}\left(1 - f_7^{tw}\right)d\gamma_{1'}^{s} + h_{1'7}^{s-tw}df_7^{tw}\gamma^{tw} \tag{6a}$$

$$d\tau_{7}^{crit} = h_{71'}^{tw-s}\left(1 - f_7^{tw}\right)d\gamma_{1'}^{s} + h_{77}^{tw-tw}df_7^{tw}\gamma^{tw} \tag{6b}$$

After integrating from A to A' (marked in Fig. 1), Equations (6a) and (6b) can be modified as the following,

$$\int_{m_{1'}\sigma_A}^{m_{1'}\sigma_{A'}} d\tau_{1'}^{crit} = h_{1'1'}^{s-s}\left(1 - f_7^{A'}\right)\int_{\gamma_{1'}^{A}}^{\gamma_{1'}^{A'}} d\gamma_{1'}^{s} + h_{1'7}^{s-tw}\gamma^{tw}\int_{f_7^{A}}^{f_7^{A'}} df_7^{tw} \tag{7a}$$

Table 5
A summary of the strain hardening coefficients determined from the experimental data.

Twin-Twin	h_{ij} (MPa)	Experiment
$h_{77}^{self-tw}$	150	$<111>_T$
h_{77}^{tw-tw} h_{1010}^{tw-tw}	1100	
$h_{710}^{tw-tw}(h_{107}^{tw-tw})$	350	
$h_{811}^{tw-tw}(h_{118}^{tw-tw})$	750	$<001>_C$
$h_{911}^{tw-tw}(h_{119}^{tw-tw})$	335	
$h_{89}^{tw-tw}(h_{98}^{tw-tw})$	210	
Slip-Twin/Twin-Slip		
$h_{7'7'}^{self-s}$	19	$<122>_T$
$h_{7'5}^{s-tw}$	55	
$h_{57'}^{tw-s}$	42	
$h_{1'7}^{s-tw}$	−90	$<144>_T$
$h_{71'}^{tw-s}$	−25	

$$\int_{m_7\sigma_A}^{m_7\sigma_{A'}} d\tau_7^{crit} = h_{71'}^{tw-s}\left(1-f_7^{A'}\right)\int_{\gamma_{1'}^{A}}^{\gamma_{1'}^{A'}} d\gamma_{1'}^{s} + h_{77}^{tw-tw}\gamma^{tw}\int_{f_7^{A}}^{f_7^{A'}} df_7^{tw} \quad (7b)$$

In the present context we take the hardening moduli $h_{1'1'}^{s-s}$ and h_{77}^{tw-tw} as the self hardening due to isolated slip and twinning, respectively, to facilitate solving for the twin-slip/slip-twin moduli.

Note that the self hardening of isolated twinning and slip can be calculated using the strain hardening slopes, i.e. $d\tau/d\gamma = m^2 d\sigma/d\varepsilon$, at the early stage of deformation in the $<111>_T$ and $<122>_T$ cases, respectively. The volume fraction of twinning at Point A′, $f_7^{A'}$, is approximated as 3.6% from the DIC strain contour. A sufficiently accurate estimate of the twin volume fraction is the areal fraction of the strain bands corresponding to twinning over the entire gauge section (see Fig. 3(a)). The shear strain of slip, $\gamma_{1'}^{s} = 5.4\%$, is given by the mean strain in the untwinned volume determined from the DIC strain contour. σ_A and $\sigma_{A'}$ are extracted from the stress-strain curve of the $<144>_T$ case (Fig. 1) as 350 MPa and 340 MPa, respectively. Solving Equations (7a) and (7b) with these parameters, we obtain $h_{1'7}^{s-tw}$ as −90 MPa and $h_{71'}^{tw-s}$ as −15 MPa. Following the same method, we calculated the hardening moduli corresponding to the twin-twin cases. The detailed calculation procedure has been demonstrated elsewhere [42]. The resulting h_{ij} values from different interactions are listed in Table 5. It is important to note that $h_{77}^{self-tw}$ and $h_{7'7'}^{self-s}$ denote the self hardening due to an isolated twin and an isolate slip system. In the case of twinning, we found that $h_{77}^{self-tw}$ is significantly smaller than the self-hardening moduli, h_{77}^{tw-tw} and h_{1010}^{tw-tw}, when both primary and latent systems are present. Under the same scenario, it is also evident that the latent hardening moduli are smaller than the self hardening moduli.

3.5. Prediction of the flow stress based on the calculated coefficients at different strain levels

Depending on the specific twin or slip system, the corresponding modified flow stress due to twin-twin and slip-twin/twin-slip interactions at certain shear strain level can be predicted as follows,

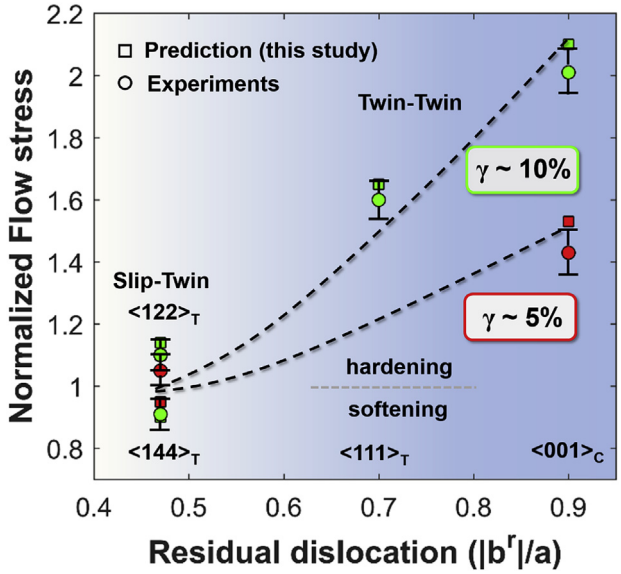

Fig. 6. The normalized flow stress as a function of residual dislocation magnitude for each crystal orientation, where slip-twin interactions are observed for $<144>_T$ and $<122>_T$ cases and twin-twin interactions for $<111>_T$ and $<001>_C$ cases. The dashed lines are guides for the eye.

$$\tau_i^{tw} = \tau_i^{N-tw} + h_{ii}^{self-tw}\gamma_i^{tw} + \sum_j h_{ij}^{tw-tw}\gamma_j^{tw} + \sum_k h_{ik}^{tw-s}\gamma_k^{s} \quad (8a)$$

$$\tau_i^{s} = \tau_i^{N-s} + h_{ii}^{self-s}\gamma_i^{s} + \sum_i h_{ij}^{s-s}\gamma_j^{s} + \sum_k h_{ik}^{s-tw}\gamma_k^{tw} \quad (8b)$$

where τ_i^{N-tw} is the critical resolved shear stress of twinning, and τ_i^{N-s} is the critical resolved shear stress of slip. Using the experimentally determined strain hardening coefficients, we calculate the modified flow stress for a specific slip or twin system based on Equations (8a) and (8b) at different shear strains, i.e. $\gamma^{tw} = \gamma^{s} \sim 5\%$ and $\gamma^{tw} = \gamma^{s} \sim 10\%$. In the $<111>_T$ and $<001>_C$ cases, the plastic deformation is predominately accommodated by twin activities. Therefore, the predicted flow stress for the i-th twin system is carried out without considering the contribution of twin-slip interaction, i.e. the fourth term in Equation (8a) is omitted. Similarly, the contribution of slip-slip interaction, i.e. the third term in Equation 8b, is omitted in the $<144>_T$ and $<122>_T$ case due to the dominant slip-twin interaction. Fig. 6 illustrates the variation of the normalized flow stress, $\tau_i^{tw}/\tau_i^{N-tw}$ or τ_i^{s}/τ_i^{N-s}, for each crystal orientation as a function of the corresponding residual Burgers vector. It is important to note that the normalized flow stress tends to increase with increasing $|\underline{b}^r|$ (see Section 4.2 for further discussion) and the agreement between predictions and experimental results is very good at both strain levels. The simultaneous nucleation of three twin systems in the $<001>_C$ case leads to three pairs of mutual interactions. Therefore, the residual Burgers vector in Fig. 6 for the $<001>_C$ case is an averaged value of the $|\underline{b}^r|$ listed in Table 4. Similarly, the corresponding normalized flow stress shown in Fig. 6 for this case is an average of $\tau_8^{tw}/\tau_8^{N-tw}$, $\tau_9^{tw}/\tau_9^{N-tw}$ and $\tau_{11}^{tw}/\tau_{11}^{N-tw}$. Following the same procedure, for slip-twin and twin-slip interactions ($<144>_T$ and $<122>_T$) the normalized flow stresses are calculated separately for the observed slip and twin

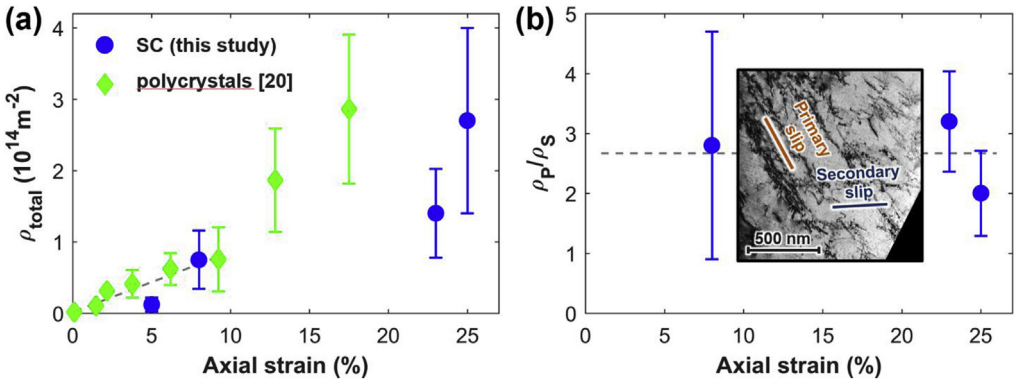

Fig. 7. (A) Increase of total dislocation density and (b) ratio of density on primary to secondary slip system depending on axial strain in FeMnNiCoCr at 77 K. The TEM image in (b) shows an example for slip-slip interaction. SC stands for single crystal. Dashes indicate the linear approximations used to model the dislocation density in Section 4.3.

systems and the averaged values are presented in Fig. 6 against $|\underline{b}^r|$.

4. Discussion

It has been shown that twinning can have both hardening and softening effects on the stress-strain behavior [10,48,49]. Hardening (as well as strengthening) related to twinning is caused by both a reduction of the mean free distance for dislocations travelling through the parent crystal (dynamic Hall-Petch behavior) as well as the conversion of former glissile dislocations into sessiles by the twinning shear (Basinski mechanism [47]). On the other hand, the detailed mechanisms leading to softening upon deformation twinning have not been unanimously resolved, especially in light of the present findings as laid out below.

4.1. Critical twin stress

The stress-strain response of the <144>$_T$ oriented single crystal showed a decrease in the stress with an increment of strain up to approximately 10% axial strain. Hitherto, twinning-induced strain softening has been attributed generally to the lattice reorientation by the twinning shear [48,49]. Lattice reorientation produces favorable (i.e. high) SFs on slip systems inside the twinned volumes, which in the formerly untwinned state were oriented unfavourably (i.e. exhibited low SFs). This type of twin-related geometric softening has been observed at high strains >10% in hcp alloys and metals. Important to note is that despite geometric softening the overall net stress-strain slope recorded in these cases has been positive, thus albeit at a lower rate hardening persisted when geometric softening was present. The underlying reason is the dominance of hardening effects (dynamic Hall-Petch and Basinski hardening) surpassing softening in those cases.

By contrast, softening for the <144>$_T$ orientation in the present study (Fig. 1) dominates, i.e. surpasses hardening, and occurs at very low axial plastic strain (<0.2%) immediately after yielding to ~10% axial strain. These observations suggest a mechanism different from geometric softening engenders the experimentally observed gradual stress decrease for <144>$_T$. This idea is further confirmed by the small orientation changes evidenced by EBSD.

Net softening is commonly observed at the yield point in BCC alloys and metals containing interstitial impurities and manifests as a distinct sudden load drop giving rise to discontinuous yielding. Softening in these systems arises from the combined effect of dislocation unpinning, rapid dislocation multiplication and the stress dependence of the dislocation velocity [50]. This mechanism

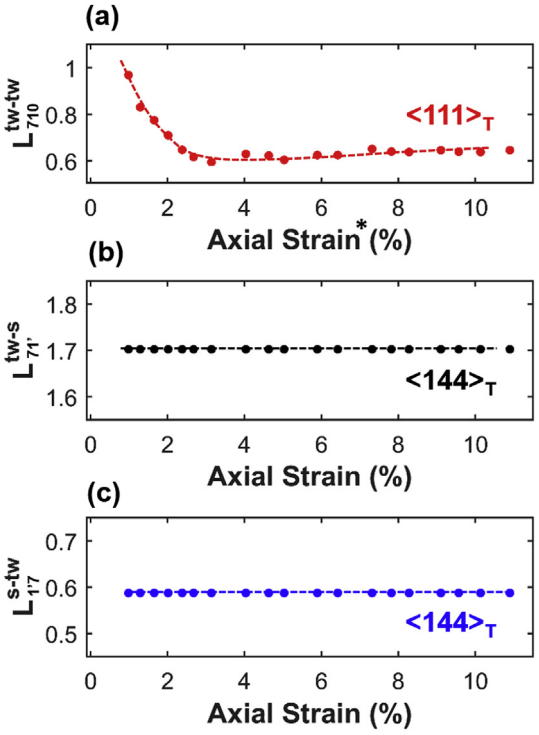

Fig. 8. LHR for different deformation mechanisms: (a) twin-twin interaction observed in <111>$_T$ case, (b) twin-slip interaction observed in <144>$_T$ case and (c) slip-twin interaction observed in <144>$_T$ case. * Note that the axial strain presented for the twin-twin case in <111>$_T$ is offset by ~9% of strain which is mainly accommodated by the primary twin system prior to activation of the second twin system. Dashes show the overall trends.

can result in serrated yielding (Portevin-le Chatelier effect) in both BCC and FCC materials, however in a less distinctive manner in FCC than in BCC [51].

Phenomenologically similar to the Portevin-le Chatelier effect though based on a physically different mechanism, serrated yielding of FCC materials at low temperature can be caused by the destabilization and breakdown of Lomer-Cottrell locks at the tips of edge dislocations pile-ups, a behavior which is closely related to the reduced mobility of screw dislocations at low temperature [52].

While the above examples give rise to net load drops, dislocation activity, their multiplication and interaction in the absence of

twinning leads generally to hardening when the overall forest dislocation density ρ_{total} increases as described by Taylor's empirical relation [53,54].

$$\tau^s = \tau^{N-s} + \alpha\mu b\sqrt{\rho_{total}} \tag{9}$$

where μ and α are the shear modulus and a dimensionless positive material constant, respectively. As plastic strain via slip accumulates dislocations multiply and ρ_{total} increases. FeMnNiCoCr follows this trend as demonstrated in Fig. 7(a). The dislocation density labeled 'this study' was estimated from TEM images of the available single crystal orientations in the present and our previous work [42]. Likewise, the total dislocation density for $<144>_T$ grows with applied strain, yet, despite accruing dislocations $<144>_T$ displays net flow softening <10% axial strain. While their overall density increases, the ratio of dislocations on the primary vs. the secondary slip system stays roughly constant as illustrated in Fig. 7(b).

The present results demonstrate a phenomenon clearly different from slip based softening (discontinuous and serrated yielding) as evidenced by the absence of an abrupt load drop which is instead replaced by continuous softening over several % strain. Furthermore, the twin related softening mechanism for $<144>_T$ incontrovertibly dominates the stress response surpassing the sum of Taylor hardening (Equation (9)) and twin-slip/slip-twin latent hardening.

The observation of the twin migration stress in $<144>_T$ point to two important findings. First, the twin migration stress can be less than the twin nucleation stress despite slip interacting with the twin boundaries, which is manifested by the continuous load decrease. Second, at high strains (stresses) when twin-twin interactions are expected to dominate, the twin migration stress is elevated. This is evident in the $<111>_T$ and $<001>_C$ compression experiments. Since the mechanical response at large strains is dictated by such interactions, the overall deformation response may not conform to Schmid's law after all. This departure from Schmid's law has consequences for the formulation of flow criteria and the flow rule for FCC alloys. Any successful theory for the work-hardening of FCC alloys will have to accurately incorporate the hardening and softening contributions from individual interactions between slip and twin systems.

Another aspect worth recalling is the stronger strain localization for $<144>_T$ than for other orientations (Fig. 3). Pronounced strain localization is invariably connected to low hardening or softening (e.g. Lüders bands in crystalline materials, necking, shear bands in metallic glasses) and the present observations agree with this notion.

4.2. The role of residual dislocations

Several papers [6,22,25,55–57] have been devoted to reactions and possible outcomes of dislocations interacting with different types of twin/grain boundaries utilizing experimental methods and atomistic simulations. On experimental grounds three conditions have been proposed to explain the tendency for a dislocation to transmit across a grain boundary [44,58]. The entirety of these studies demonstrate that dislocation-interface reactions are highly complex processes governed by numerous factors across all length scales, from the macroscopic stress state to the boundary geometry to subatomic energy landscapes. However, pre-eminent is the role taken by the residual dislocations $\underline{b}^r$ created during the reaction at the point of interaction and the importance of $\underline{b}^r$ for the hardening characteristics of interfaces impeding slip has been unanimously illustrated [5,6,24].

In the current work it was possible to deduce the strong influence of $\underline{b}^r$ from experiments. As shown in Section 3.3, steeper hardening is associated with larger $|\underline{b}^r|$ and, therefore, slip-twin interactions, which in general produce relatively smaller $|\underline{b}^r|$ than twin-twin interactions, lead to weaker hardening than twin-twin mechanisms. Consequently, for sufficiently small $|\underline{b}^r|$ zero hardening or even net softening may entail as exhibited in the $<144>_T$ experiment.

4.3. The form of the hardening law and latent hardening ratio

It is important to note that the strengthening of a material due to slip and twin can also be related to its dislocation density (Taylor's classical relation [53]) and twin volume fraction (Remy's model [16]), respectively. The mathematical form for the stress increase combining different hardening mechanisms, in particular for slip-slip interactions, has been debated [35, 60, 61]. Franciosi et al. [34] verified that the use of a quadratic (vs. a linear) relation results in better agreement with the experimental latent hardening results. Therefore, we propose a similar procedure where the squares of each contribution to the flow stress are added up. Consequently, the hardening on the system j can be expressed as

$$\Delta\tau_j = \mu b\sqrt{\sum_k \left(\alpha_{jk}^{s-s}\right)^2\rho_k + \sum_k \left(\overline{\alpha}_{jk}^{s-tw}\bar{f}_k\right)^2 + \sum_k \left(\alpha_{jk}^{tw-s}\right)^2\rho_k + \sum_k \left(\overline{\alpha}_{jk}^{tw-tw}\bar{f}_k\right)^2} \tag{10}$$

where μ is the elastic shear modulus, b is the magnitude of the Burgers vector, ρ_k is the dislocation density on system k, and α_{jk} define the interaction strength between two deformation systems. For pairs of slip systems α_{jk}^{s-s} ranging from 0.04 to 0.72 were reported [62, 63] but values for twin-related interactions are vague [16]. $\overline{\alpha}_{jk}^{s-tw}$ and $\overline{\alpha}_{jk}^{tw-tw}$ are the products of the Schmid factor (m_k) and the interaction coefficients ($\alpha_{jk}^{s-tw}$and α_{jk}^{tw-tw}). The superscript '2' in Equation (10) indicates squares of matrix elements (i.e. of scalar quantities). $\bar{f}_k$ can be written as $(2t_k)^{-1}\frac{f_k}{1-f_k}$ [16], where t_k is the twin thickness and f_k is the twin volume fraction. Note that t_k, f_k and ρ_k are based on the present experiments at different strain levels and are found to evolve almost linearly with axial strain between 0% and 10% (as e.g. indicated for ρ_{total} in Fig. 7(a)).

Direct application of Equation (10) to predict the change of flow stress accurately can be rather difficult as the determination of the interaction coefficients can be very intricate in cases where multiple systems are active. Nevertheless, it allows us obtaining estimates for the latent hardening ratio (LHR), which can give important insight into the evolution of the ratio between h_{jk} ($k \neq j$) and h_{kk} as a function of strain. Based on the LHR for the slip-slip case L_{ji}^{s-s} (Equation (11) [34]), we extend this concept to twin-related interactions. In this manner, the LHR for slip-twin (L_{ji}^{s-tw}), twin-slip (L_{ji}^{tw-s}) and twin-twin (L_{ji}^{tw-tw}) cases can be presented as

$$L_{ji}^{s-s} = \frac{\Delta\tau_j}{\Delta\tau_i} = \left\{ \frac{\left(\alpha_{ji}^{s-s}\right)^2 \rho_i + \left[C_L - \left(\alpha_{ji}^{s-s}\right)^2 \rho_i\right]}{\left(\alpha_{ii}^{s-s}\right)^2 \rho_i + \left[C_P - \left(\alpha_{ii}^{s-s}\right)^2 \rho_i\right]} \right\}^{1/2}$$
$$C_L = \sum_k \left(\alpha_{jk}^{s-s}\right)^2 \rho_k \qquad (11)$$
$$C_P = \sum_k \left(\alpha_{ik}^{s-s}\right)^2 \rho_k$$

$$L_{ji}^{s-tw} = \left\{ \frac{\left(\alpha_{ji}^{s-tw}\bar{f}_i\right)^2 + \left[C_L - \left(\alpha_{ji}^{s-tw}\bar{f}_i\right)^2\right]}{\left(\alpha_{ii}^{self-tw}\bar{f}_i\right)^2 + \left[C_P - \left(\alpha_{ii}^{self-tw}\bar{f}_i\right)^2\right]} \right\}^{1/2}$$
$$C_L = \sum_k \left(\alpha_{jk}^{s-tw}\bar{f}_k\right)^2 + \sum_m \left(\alpha_{jm}^{s-s}\right)^2 \rho_m \qquad (12)$$
$$C_P = \sum_k \left(\alpha_{ik}^{tw-s}\right)^2 \rho_k + \sum_m \left(\alpha_{im}^{tw-tw}\bar{f}_m\right)^2$$

$$L_{ji}^{tw-s} = \left\{ \frac{\left(\alpha_{ji}^{tw-s}\right)^2 \rho_i + \left[C_L - \left(\alpha_{ji}^{tw-s}\right)^2 \rho_i\right]}{\left(\alpha_{ii}^{self-s}\right)^2 \rho_i + \left[C_P - \left(\alpha_{ii}^{self-s}\right)^2 \rho_i\right]} \right\}^{1/2}$$
$$C_L = \sum_k \left(\alpha_{jk}^{tw-s}\right)^2 \rho_k + \sum_m \left(\alpha_{jm}^{tw-tw}\bar{f}_m\right)^2 \qquad (13)$$
$$C_P = \sum_k \left(\alpha_{ik}^{s-tw}\bar{f}_k\right)^2 + \sum_m \left(\alpha_{im}^{s-s}\right)^2 \rho_m$$

$$L_{ji}^{tw-tw} = \left\{ \frac{\left(\alpha_{ji}^{tw-tw}\bar{f}_i\right)^2 + \left[C_L - \left(\alpha_{ji}^{tw-tw}\bar{f}_i\right)^2\right]}{\left(\alpha_{ii}^{tw-tw}\bar{f}_i\right)^2 + \left[C_P - \left(\alpha_{ii}^{tw-tw}\bar{f}_i\right)^2\right]} \right\}^{1/2}$$
$$C_L = \sum_k \left(\alpha_{jk}^{tw-tw}\bar{f}_k\right)^2 \qquad (14)$$
$$C_P = \sum_k \left(\alpha_{ik}^{tw-tw}\bar{f}_k\right)^2$$

Fig. 8 illustrates the evolution of the corresponding LHR for twin-twin, twin-slip, and slip-twin interactions with axial strain (0%–10%) using Equations (12)–(14), respectively. To facilitate the calculation, the interaction coefficients, α_{jk}, are approximated by the hardening moduli, h_{jk}, listed in Table 5. Note that the LHR in the case of twin-twin first decreases with increasing strain and eventually saturates at a value of ~0.6, while the variation with strain for slip-twin and twin-slip is negligible, that is to say they are constant at ~0.59 and ~1.7, respectively. The fact that the LHR in the twin-twin case becomes 0.6 after 3% strain implies that the latent hardening is smaller than self hardening. This result is consistent with the moduli presented in Table 5 and Wu et al. [29]. In the case of slip-slip interaction, the ratio between the dislocation density on the primary system (ρ_p) to that on the secondary system (ρ_s) is approximately constant at ~2.8, as shown in Fig. 7(b). The corresponding slip-slip LHR is ~0.65 according to Equation (11).

To demonstrate the calculation the slip-twin interaction for the case of <144>$_T$ is utilized. In this case, the interaction between slip system 1′ and twin system 7 was revealed (see Fig. 1). Therefore, Equation (12) can be further simplified to

$$L_{1'7}^{s-tw} = \left[\frac{\left(\alpha_{1'7}^{s-tw}\right)^2 \frac{\bar{f}_2^2}{\rho_{1'}} + \left(\alpha_{1'1'}^{self-s}\right)^2}{\left(\alpha_{77}^{self-tw}\right)^2 \frac{\bar{f}_2^2}{\rho_{1'}} + \left(\alpha_{71'}^{tw-s}\right)^2} \right]^{1/2} \qquad (15)$$

We like to point out that Equation (15) implies that the change of the slip-twin LHR is strongly affected by the variation of $\bar{f}_2^2/\rho_{1'}$ with strain. However, such variation is rather small in <144>$_T$ resulting in a constant LHR (Fig. 8(c)).

5. Conclusions

The most important outcomes of this study are:

(i) Twin-twin interactions impart higher hardening levels than slip-twin and twin-slip interactions. While slip-twin and twin-slip interaction are associated with low hardening or even softening, twin–twin interactions give rise to pronounced hardening. The degree of hardening is reflected in the attendant hardening moduli, which take both negative and positive values for slip-twin and twin-slip, but more than 10 times larger positive values for twin-twin.

(ii) The magnitude $|\underline{b}^r|$ of residual Burgers vectors for slip-twin and twin-twin interactions are indicative for the expected level of hardening. Higher $|\underline{b}^r|$ are associated with stronger hardening while limited hardening observed for small $|\underline{b}^r|$ can lead to net softening.

(iii) Transmission electron microscopy (TEM) supports the occurrence of twin-slip/slip-twin and twin-twin interactions in the single crystals studied in uniaxial experiments. Aside from partial dislocations separated by intrinsic stacking faults, a large part of lattice dislocations are full dislocations of type $\frac{a}{2}<011>$.

(iv) The increase in flow stress beyond the yield point can be accurately predicted by a mesoscale formulation incorporating hardening by slip-slip, slip-twin, twin-slip and twin-twin interactions. Future polycrystal hardening laws will benefit from including these contributions into their framework.

Acknowledgements

The work is supported by NSF-CMMI 1562288 which is gratefully acknowledged. We would like to thank Prof. Yuri Chumlyakov of Tomsk State University, Russia for providing the single crystals. TEM and EBSD analyses were carried out in part in the Frederick Seitz Materials Research Laboratory Central Research Facilities, University of Illinois.

Appendix A

Fig. A1(a) illustrates a Burgers vector analysis for a set of lattice dislocations on $(\bar{1}11)$ in front of a $(1\bar{1}1)$ twin boundary using the $\underline{g}.\underline{b} = 0$ invisibility criterion [59]. Prior identification of the slip plane reduces the number of candidate Burgers vectors to 3 full dislocations and partials each. The images shown were recorded in two-beam bright-field condition with 3 different $\underline{g}$ vectors. For $\underline{g} = (022)$ invisibility occurs and, thus, the investigated dislocations are full dislocations with Burgers vector $\underline{b} = \pm[0\bar{1}1]$. The character of the full dislocations in Fig. A1(a) is further corroborated by the absence of stacking faults in their vicinity. In addition to full dislocations, the presence of partials is inferred from occasional stacking faults such as in Fig. A1(b). The variation of its fringe contrast in the $\underline{g} = (\bar{2}20)$ bright-field dark-field image pair reveals its nature (intrinsic vs. extrinsic) as intrinsic [59].

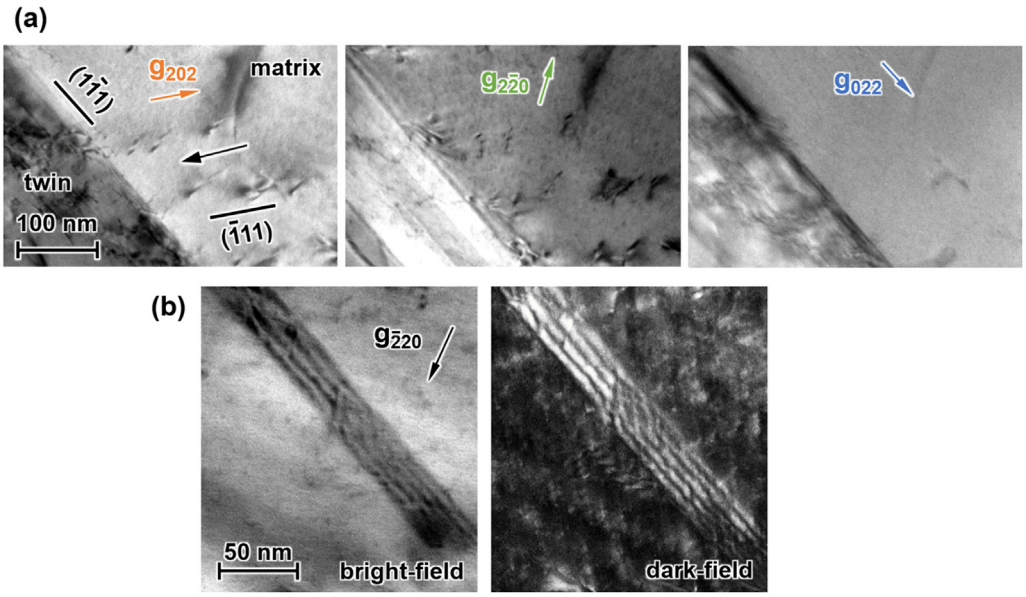

Fig. A1. (a) Burgers vector analysis of full lattice dislocations ahead of a $(1\bar{1}1)$ twin boundary by two-beam bright-field images. The black arrow indicates the assumed direction of movement. (b) Bright-field dark-field pair of an intrinsic stacking fault. The imaging reflection is indicated in each panel.

References

[1] T. Blewitt, R. Coltman, J. Redman, Low-temperature deformation of copper single crystals, J. Appl. Phys. 28 (1957) 651–660.
[2] L. Remy, Twin-twin interaction in FCC crystals, Scripta Metall. 11 (1977) 169.
[3] L. Remy, The interaction between slip and twinning systems and the influence of twinning on the mechanical behavior of fcc metals and alloys, Metall. Mater. Trans. 12 (1981) 387–408.
[4] Z.H. Jin, P. Gumbsch, K. Albe, E. Ma, K. Lu, H. Gleiter, et al., Interactions between non-screw lattice dislocations and coherent twin boundaries in face-centered cubic metals, Acta Mater. 56 (2008) 1126.
[5] T. Ezaz, M.D. Sangid, H. Sehitoglu, Energy barriers associated with slip-twin interactions, Phil. Mag. 91 (2010) 1464–1488.
[6] M.D. Sangid, T. Ezaz, H. Sehitoglu, Energetics of residual dislocations associated with slip–twin and slip–GBs interactions, Mater. Sci. Eng. 542 (2012) 21–30.
[7] Y. Zhu, X. Wu, X. Liao, J. Narayan, L. Kecskes, S. Mathaudhu, Dislocation–twin interactions in nanocrystalline fcc metals, Acta Mater. 59 (2011) 812–821.
[8] L. Lu, Y. Shen, X. Chen, L. Qian, K. Lu, Ultrahigh strength and high electrical conductivity in copper, Science 304 (2004) 422–426.
[9] M. Dao, L. Lu, Y.F. Shen, S. Suresh, Strength, strain-rate sensitivity and ductility of copper with nanoscale twins, Acta Mater. 54 (2006) 5421.
[10] I. Karaman, H. Sehitoglu, A.J. Beaudoin, Y.I. Chumlyakov, H.J. Maier, C.N. Tome, Modeling the deformation behavior of Hadfield steel single and polycrystals due to twinning and slip, Acta Mater. 48 (2000) 2031–2047.
[11] I. Kireeva, Y.I. Chumlyakov, Z. Pobedennaya, Y.N. Platonova, I. Kuksgauzen, D. Kuksgauzen, et al., Slip and twinning in the [1 49]-oriented single crystals of a high-entropy alloy, Russ. Phys. J. 59 (2016) 1242–1250.
[12] Y.M. Wang, F. Sansoz, T. LaGrange, R.T. Ott, J. Marian, T.W. Barbee Jr., et al., Defective twin boundaries in nanotwinned metals, Nat. Mater. 12 (2013) 697.
[13] A. Stukowski, K. Albe, D. Farkas, Nanotwinned fcc metals: strengthening versus softening mechanisms, Phys. Rev. B 82 (2010) 224103.
[14] X. Li, Y. Wei, L. Lu, K. Lu, H. Gao, Dislocation nucleation governed softening and maximum strength in nano-twinned metals, Nature 464 (2010) 877.
[15] I. Karaman, H. Sehitoglu, K. Gall, Y.I. Chumlyakov, H.J. Maier, Deformation of single crystal Hadfield steel by twinning and slip, Acta Mater. 48 (2000) 1345.
[16] L. Remy, Kinetics of fcc deformation twinning and its relationship to stress-strain behaviour, Acta Metall. 26 (1978) 443–451.
[17] P. Chowdhury, H. Sehitoglu, W. Abuzaid, H.J. Maier, Mechanical response of low stacking fault energy Co–Ni alloys – continuum, mesoscopic and atomic level treatments, Int. J. Plast. 71 (2015) 32–61.
[18] A. Zaddach, C. Niu, C. Koch, D. Irving, Mechanical properties and stacking fault energies of NiFeCrCoMn high-entropy alloy, JOM (J. Occup. Med.) 65 (2013) 1780–1789.
[19] F. Otto, A. Dlouhý, C. Somsen, H. Bei, G. Eggeler, E.P. George, The influences of temperature and microstructure on the tensile properties of a CoCrFeMnNi high-entropy alloy, Acta Mater. 61 (2013) 5743–5755.
[20] G. Laplanche, A. Kostka, O. Horst, G. Eggeler, E. George, Microstructure evolution and critical stress for twinning in the CrMnFeCoNi high-entropy alloy, Acta Mater. 118 (2016) 152–163.
[21] W. Abuzaid, H. Sehitoglu, Critical resolved shear stress for slip and twin nucleation in single crystalline FeNiCoCrMn high entropy alloy, Mater. Char. 129 (2017) 288–299.
[22] L. Patriarca, W. Abuzaid, H. Sehitoglu, H.J. Maier, Slip transmission in bcc FeCr polycrystal, Mater. Sci. Eng. 588 (2013) 308–317.
[23] P. Chowdhury, H. Sehitoglu, R. Rateick, Recent advances in modeling fatigue cracks at microscale in the presence of high density coherent twin interfaces, Curr. Opin. Solid State Mater. Sci. 20 (2016) 140–150.
[24] P. Chowdhury, H. Sehitoglu, H. Maier, R. Rateick, Strength prediction in NiCo alloys–the role of composition and nanotwins, Int. J. Plast. 79 (2016) 237–258.
[25] M.D. Sangid, T. Ezaz, H. Sehitoglu, I.M. Robertson, Energy of slip transmission and nucleation at grain boundaries, Acta Mater. 59 (2011) 283–296.
[26] Z.X. Wu, Y.W. Zhang, D.J. Srolovitz, Dislocation-twin interaction mechanisms for ultrahigh strength and ductility in nanotwinned metals, Acta Mater. 57 (2009) 4508.
[27] Friedel J. Commentary, in: F.R.N. Nabarro, M.S. Duesbery (Eds.), Dislocations in Solids, Elsevier, 2002 xix-xxiii.
[28] B.C. De Cooman, Y. Estrin, S.K. Kim, Twinning-induced plasticity (TWIP) steels, Acta Mater. 142 (2018) 283–362.
[29] T.-Y. Wu, J.L. Bassani, C. Laird, Latent hardening in single crystals I. Theory and experiments, Proc. Roy. Soc. Lond.: Mathematical, Physical and Engineering Sciences: The Royal Society (1991) 1–19.
[30] J. Mandel, Generalisation de la theorie de plasticite de W. T. Koiter, Int. J. Solid Struct. 1 (1965) 273–295.
[31] R. Hill, Generalized constitutive relations for incremental deformation of metal crystals by multislip, J. Mech. Phys. Solid. 14 (1966) 95–102.
[32] M. Cherkaoui, Constitutive equations for twinning and slip in low-stacking-fault-energy metals: a crystal plasticity-type model for moderate strains, Phil. Mag. 83 (2003) 3945–3958.
[33] A. Salem, S. Kalidindi, S. Semiatin, Strain hardening due to deformation twinning in α-titanium: constitutive relations and crystal-plasticity modeling, Acta Mater. 53 (2005) 3495–3502.
[34] P. Franciosi, M. Berveiller, A. Zaoui, Latent hardening in copper and aluminium single crystals, Acta Metall. 28 (1980) 273–283.
[35] U. Kocks, The relation between polycrystal deformation and single-crystal deformation, Metall. Mater. Trans. B 1 (1970) 1121–1143.
[36] P. Franciosi, Glide mechanisms in bcc crystals: an investigation of the case of α-iron through multislip and latent hardening tests, Acta Metall. 31 (1983) 1331–1342.
[37] U. Kocks, T. Brown, Latent hardening in aluminum, Acta Metall. 14 (1966) 87–98.
[38] P. Jackson, Z. Basinski, Latent hardening and the flow stress in copper single crystals, Can. J. Phys. 45 (1967) 707–735.
[39] Y. Nakada, A.S. Keh, Latent hardening in iron single crystals, Acta Metall. 14 (1966) 961–973.
[40] D. Peirce, R.J. Asaro, A. Needleman, An analysis of nonuniform and localized deformation in ductile single crystals, Acta Metall. 30 (1982) 1087–1119.
[41] J. Carroll, W. Abuzaid, J. Lambros, H. Sehitoglu, An experimental methodology to relate local strain to microstructural texture, Rev. Sci. Instrum. (2010) 81.
[42] Y. Wu, M. Bönisch, A. Sertan, W. Abuzaid, H. Sehitoglu, Experimental

determination of latent hardening coefficients in FeMnNiCoCr, Int. J. Plast. 105 (2018) 239–260.
[43] S. Alkan, A. Ojha, H. Sehitoglu, Determination of latent hardening response for FeNiCoCrMn for twin-twin interactions, Acta Mater. 147 (2018) 149–164.
[44] T.C. Lee, I.M. Robertson, H.K. Birnbaum, An in Situ transmission electron microscope deformation study of the slip transfer mechanisms in metals, Metallurgical Transactions A 21 (1990) 2437.
[45] J.P.L.J. Hirth, Theory of Dislocations, McGraw Hill Book Company, 1968.
[46] S. Mahajan, G.Y. Chin, Twin-slip, twin-twin and slip-twin interactions in Co-8 wt.% Fe alloy single crystals, Acta Metallurgica 21 (1973) 173.
[47] J. Wang, I.J. Beyerlein, C.N. Tomé, An atomic and probabilistic perspective on twin nucleation in Mg, Scripta Mater. 63 (2010) 741–746.
[48] S.R. Kalidindi, A.A. Salem, R.D. Doherty, Role of deformation twinning on strain hardening in cubic and hexagonal polycrystalline metals, Adv. Eng. Mater. 5 (2003) 229–232.
[49] A.T. Churchman, The yield phenomena, kink bands and geometric softening in titanium crystals, Acta Metall. 3 (1955) 22–29.
[50] G.T. Hahn, A model for yielding with special reference to the yield-point phenomena of iron and related bcc metals, Acta Metall. 10 (1962) 727–738.
[51] E.O. Hall, Yield point Phenomena in Metals and Alloys, 1970. London: Macmillan.
[52] B. Obst, A. Nyilas, Experimental evidence on the dislocation mechanism of serrated yielding in f.c.c. metals and alloys at low temperatures, Mater. Sci. Eng. 137 (1991) 141–150.
[53] G.I. Taylor, The mechanism of plastic deformation of crystals. Part I. Theoretical, Proc. R. Soc. Lond. - Ser. A Contain. Pap. a Math. Phys. Character 145 (1934) 362–387.
[54] F.F. Lavrentev, The type of dislocation interaction as the factor determining work hardening, Mater. Sci. Eng. 46 (1980) 191–208.
[55] S. Mahajan, Twin-slip and twin-twin interactions in Mo-35 at.% Re alloy, Phil. Mag. 23 (1971) 781–794.
[56] Md Koning, R. Miller, V.V. Bulatov, F.F. Abraham, Modelling grain-boundary resistance in intergranular dislocation slip transmission, Philos. Mag. a 82 (2002) 2511–2527.
[57] W.Z. Abuzaid, M.D. Sangid, J.D. Carroll, H. Sehitoglu, J. Lambros, Slip transfer and plastic strain accumulation across grain boundaries in Hastelloy X, J. Mech. Phys. Solid. 60 (2012) 1201–1220.
[58] Z. Shen, R.H. Wagoner, W.A.T. Clark, Dislocation and grain boundary interactions in metals, Acta Metallurgica 36 (1988) 3231.
[59] D.B. Williams, C.B. Carter, Transmission Electron Microscopy - a Textbook for Materials Science, Springer, US, 2009.